



Effect of Film Thickness and Annealing on the Structural and Optical Properties of CuInAlSe₂ Thin Films

U. Parihar¹, N. Padha¹, J.R. Ray², M.S. Desai², C.J. Panchal^{2,*}, P.K. Mehta³,
 I.V. Cheshko⁴, I.Yu. Protsenko⁴

¹ Department of Physics & Electronics, University of Jammu, Jammu-180006 J & K, India

² Applied Physics Department, Faculty of Technology and Engineering, The M. S. University of Baroda, Vadodara-390001, Gujarat, India

³ Physics Department, Faculty of Science, The M. S. University of Baroda, Vadodara-390002, Gujarat, India

⁴ Applied Physics Department, Faculty of Electronic and Informational Technologies, Sumy State University, 2, Rymkogo-Korsakova Str., 40007 Sumy, Ukraine

(Received 09 July 2013; published online 31 August 2013)

CuIn_{1-x}Al_xSe₂ (CIAS) thin films were grown using flash evaporation method by varying the film thickness from 500 nm to 700 nm. Prepared CIAS thin films were annealed at 573 K for one hour in vacuum. The influence of film's thickness and the annealing temperature were characterized by the X-ray diffraction (XRD), Scanning electron microscopy (SEM), Energy dispersive analysis of X-ray (EDAX), Optical transmission measurements, and Hall Effect measurement. As the film thickness increases the crystallinity improves and due to that the optical absorption also improves. The further improvement for different thicknesses of CIAS thin films were observed by annealing. The thicker (700 nm) and annealed CIAS thin film shows the crystallite size of 24.3 nm, energy band gap of 1.19 eV, and resistivity of about $9 \times 10^2 \Omega \text{ cm}$.

Keywords: Film system, CuInAlSe₂, Optical properties, Scanning electron microscopy, Hall Effect.

PACS numbers: 61.05.C – 68.37.Lp, 78.66.Bz, 81.40.Gh

1. INTRODUCTION

Copper indium diselenide (CIS) and its alloys, CIAS and, CIASse, shows its potential towards the achievement of higher energy conversion efficiency at lower fabrication cost in the area of thin film solar cells [1, 2, 3]. The optical energy band gap of CIS increases by substituting Ga / Al for In and S for Se, which is essential to enhance the photovoltaic conversion efficiency in CIS based solar cells. For energy band gap greater than 1.3 eV the fill-factor and the open-circuit voltage of the solar cell reduces due to the degradation of the electronic properties of the absorber [4]. Aluminum (Al) is easily available and less costly compared to Gallium (Ga). By alloying of Al to CIS the energy band gap changes from 1.0 eV (CIS) to 2.7 eV (CuAlSe₂), which can absorb most of visible radiation of solar spectrum. CuIn_{1-x}Al_xSe₂ ($x = 0.13$) single junction solar cell exhibited an efficiency of 16.9 % [5]. The tandem junction was proposed [6] to achieve higher photovoltaic conversion efficiency in CuInSe₂ based solar cells as the calculated energy conversion efficiency for CIS (1.1 eV) / CIAS (1.7 eV) tandem cell was estimated to be 29 % [7]. CuIn_{1-x}Al_xSe₂ ($x = 0.13$) chalcopyrite material is prepared and CIAS thin film of different thicknesses were grown by flash evaporation method. The post-deposition annealing was carried out for the CIAS thin film of different thicknesses. The influence of the film thickness variation and the annealing temperature were observed by different methods like XRD, SEM, EDAX, optical transmission and electrical measurements.

2. EXPERIMENT

CIAS thin films were deposited by flash evaporation method on an organically cleaned, 3 mm thick, soda lime glass substrate. The CIAS compound was prepared by using the melt-quenching method, described elsewhere [8]. The substrate temperature was kept constant, at 473 K, and varied the thickness of the CIAS thin film viz. 200 nm, 500 nm and 700 nm. The deposition rate was of the order of 0.2-0.3 nm·s⁻¹ and the thickness of CIAS films was measured using a quartz crystal thickness monitor (Hind Hi Vac. DTM-101). The thermal annealing was carried out for all the different thicknesses of CIAS thin films at 573 K in rough vacuum for one hour.

All the deposited and annealed CIAS thin films were characterized using HR-X-ray diffractometer (XRD) (Bruker D8-Discover) in 2θ range 20°-70° at a scan rate 0.02 s⁻¹ with Cu-K_α radiation source. The surface morphology and chemical composition of the deposited thin films was studied using scanning electron microscope (Philips ESEM, 30XL) equipped with EDAX facilities operated at 30 kV with standard ZAF quantification.

The CIAS thin films were also characterized for optical measurement at room temperature using Hitachi U3400 UV-VIS-NIR double beam spectrophotometer. Hall measurements were done to verify the conductivity type, resistivity, mobility, and carrier concentration of the deposited thin films.

3. RESULT

3.1 Structural Characterization

There is an obtrusive betterment was clearly ob-

* cjpanchal_msu@yahoo.com

served in the XRD spectra of CIAS thin films as the film thickness increases and by annealing, as shown in Fig. 1. All the films were found to be polycrystalline in nature, majorly oriented towards (112) plane of chalcopyrite structure. Since no PDF-ICDD data file is available for $\text{Cu}(\text{In}, \text{Al})\text{Se}_2$, we used Copper indium diselenide (CuInSe_2) as the standard data [9]. Detailed study of crystal structure and phase composition of Fe and Au thin films was done in earlier studies. It allowed us to pick deposition conditions so that all components of systems have a crystalline structure and have not oxide phases.

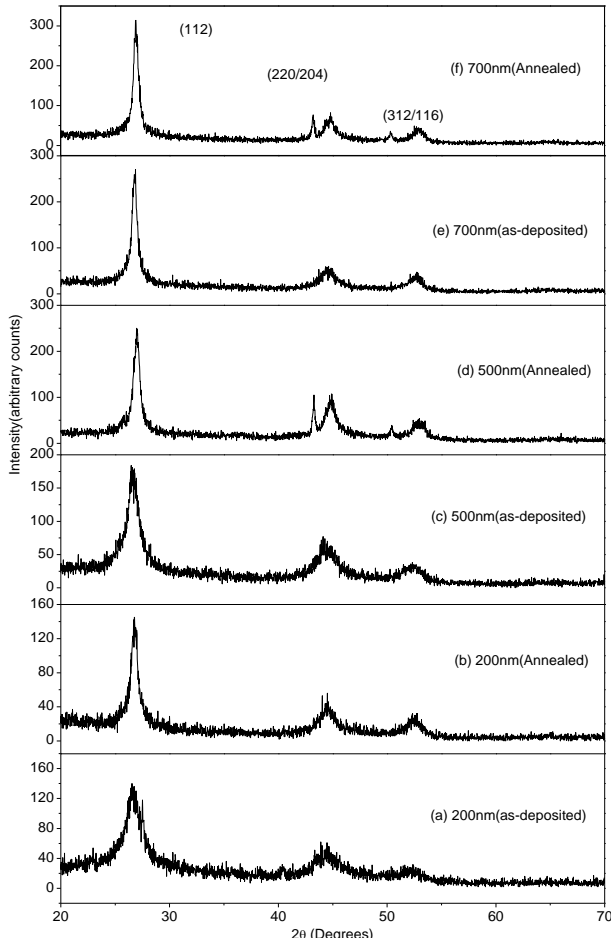


Fig. 1 – The XRD pattern of the prepared CIAS thin films at different thicknesses (a) 200 nm (as-deposited), (b) 200 nm (annealed), (c) 500 nm (as-deposited), (d) 500 nm (annealed) (e) 700 nm (as-deposited) and (f) 700 nm (annealed)

The XRD spectra suggest that the crystallinity increases with increase in the thickness of the CIAS thin film. As the films thickness increases the intensity of (112) diffraction peak increases and the shape of the diffraction peak sharpens. The strain decreases with the increase of film thickness, which reflects the decrease in the cohesive force between film and substrate material. Therefore, we conclude that there is a decrease in the lattice imperfections with increase in film thickness and an increase in the crystallite size [10].

The average crystalline size (D) of all the deposited CuInAlSe_2 thin films was evaluated from the XRD peak along (112) orientation by using Scherer's relation [11]

$$D = \frac{0.9\lambda}{\beta \cos \theta} \quad (1)$$

where D is the crystallite size as measured perpendicular to the reflecting plane, 0.9 is the Scherer's constant, λ is the wavelength of the X-ray radiation, β is the full width at half the maximum intensity, and θ is the Bragg's angle. Various other structural parameters viz. dislocation density (δ), micro strain (ϵ), and the estimated number of crystallites (N) were observed [12] as a function of thickness have also been calculated using relevant formulae and are presented in Table 1.

The film with thickness 200 nm showed a large FWHM because of the large misfit strain between the film and the substrate. Its value decreased gradually as the thickness of CIAS thin film increases. This result is attributed to the relaxation of the mismatch strain with the formation of misfit dislocation in the films [13]. Therefore, as the film thickness increases, the misfit strain decreases resulting in a better crystallinity. The annealed films also showed a decrease in the value of FWHM and an increase in the intensity as compared to the as-deposited films.

3.2 Morphological Studies

The surface morphologies of the CIAS films deposited at different substrate temperatures have been studied by using scanning electron microscope (SEM). Fig. 2 shows the SEM images of the surface morphology of the CIAS thin films as-deposited as well as annealed at 573 K in rough vacuum, having different thicknesses. It is observed that the surface morphology of the CIAS thin films varies with thickness as well as with annealing. For small thickness, SEM images present small nucleation sites because of the short time of growth. However, as the thickness increases, the grain size increases, and the film morphology seems to be uniform with large grains. From the fundamental structure-forming phenomenon, film growth evolves from nucleation islands to the growth of the continuous films, leading to large grains formed by the coalescence phenomenon between grains [14].

3.3 Compositional Analysis

In order to verify the composition of the deposited films, their compositional analysis has been made by using EDAX characterization. The values of the constituent elements so obtained are presented in Table 2. At lower CIAS film thickness, there has been a deficiency of selenium, which is due to its highly volatile nature and leads to degradation of the quality of the film [15]. However, the selenium composition is the key factor for device applications of undertaken films.

Further, with the increment in the thickness of the film an improvement of selenium content in the film is observed and demonstrated its improved quality. It is seen that up to 500 nm we have observed the Cu-rich composition, however, as the thickness is increased to 700 nm, the ratio of $\text{Cu} / (\text{In} + \text{Al})$ was found to be about 0.73, i.e. Cu atoms are relatively small compared to $(\text{In} + \text{Al})$ while the ratio of $(\text{Cu} + \text{In} + \text{Al}) / \text{Se}$ is close to unity. Since Cu-poor surface is beneficial for the overall

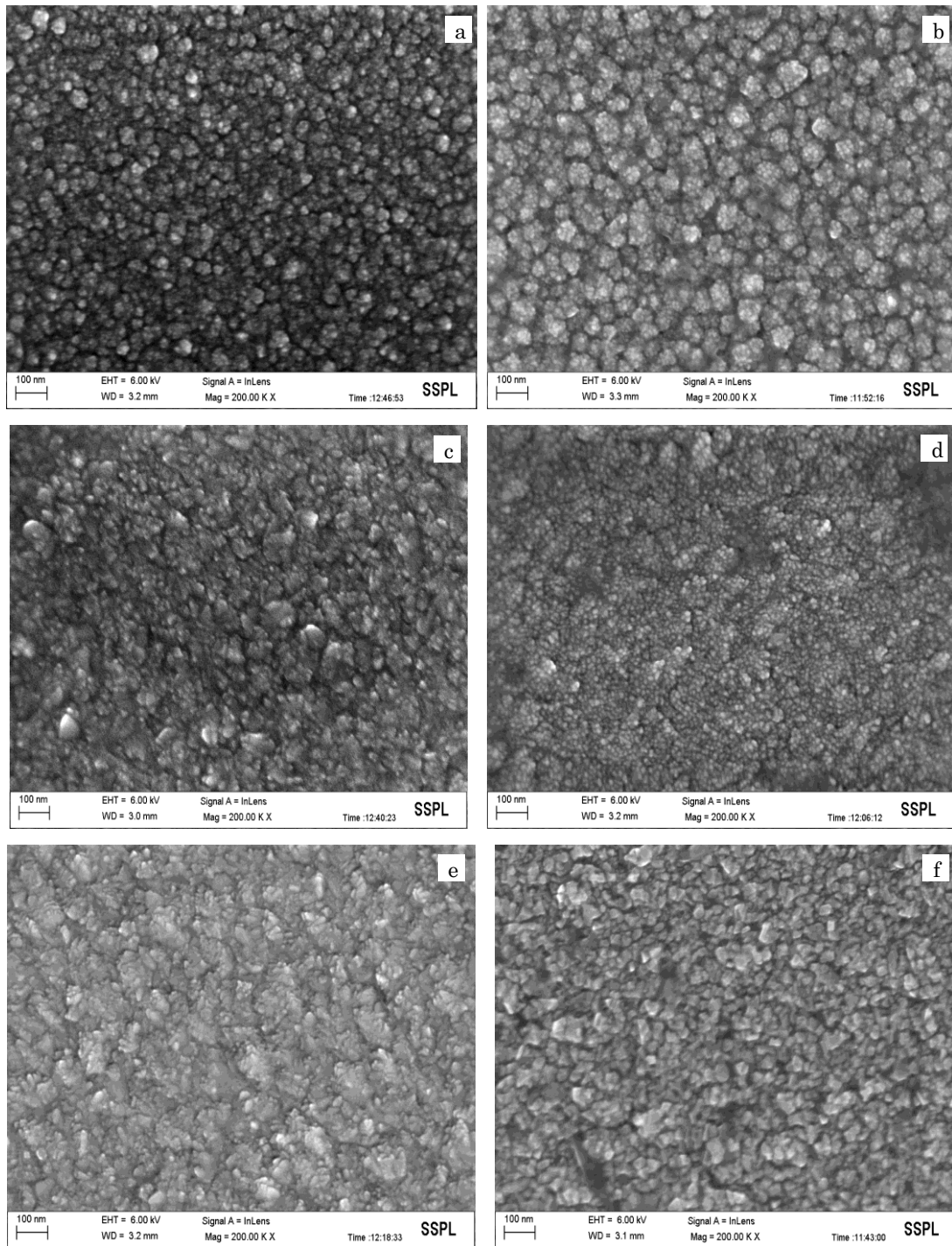


Fig. 2 – SEM micrographs of flash evaporated CIAS thin films of different thickness (a) 200 nm (as-deposited), (b) 200 nm (annealed), (c) 500 nm (as-deposited), (d) 500 nm (annealed), (e) 700 nm (as-deposited), and (f) 700 nm (annealed)

Table 1 – Significant parameters obtained from XRD analysis

Thickness (nm)	Sample type	FWHM (degree)	Crystallite size, D (nm)	Micro Strain, ϵ	Dislocation Density ($\times 10^{10}$ Lines/m ²)	Inter-planar Spacing, d (nm)	No. of Crystallites N (1×10^{14})
200	As-deposited	0.576	14.8	0.0024	0.00456	0.335	616.94
200	Annealed	0.432	19.7	0.0018	0.00257	0.332	260.40
500	As-deposited	0.513	16.6	0.0021	0.00363	0.336	1095.04
500	Annealed	0.422	20.2	0.0017	0.00244	0.329	604.82
700	As-deposited	0.399	21.4	0.0016	0.00219	0.332	717.27
700	Annealed	0.351	24.3	0.0014	0.00169	0.331	488.44

performance of the film for device application [16]. Further, it has been noted that annealing of the films improves their quality. However, thickness beyond 700 nm caused re-evaporation of selenium, thus, confirming 700 nm thick film suits to various device applications.

3.4 Optical Characterization

The optical transmission spectra of CIAS thin films with varying thicknesses have been shown in Fig. 3. The higher transmittance indicates a smooth surface and relatively good homogeneity of the thinner films and their results are consistent with the results of SEM analysis [17]. The transmittance of the films was found to decrease and absorbance was found to increase with increase in thickness. This is because of the reason that in case of thicker films more atoms are present in the film; thus, make more states available for the photons to get absorbed, thereby, increasing the absorbance of films with increasing thicknesses [18]. However, with the increase of film thickness, the scattering of the light also increases thus causing a loss to the coherence between the primary light beam and the beam reflected between the film boundaries and results in the disappearance of the interference as well as reduction of the transmittance [18].

The optical band gap E_g is estimated by using the following relation [19],

$$ahv = B(hv - E_g)^m \quad (2)$$

where B is a constant, E_g is the band gap energy, $h\nu$ is the incident photon energy and m a constant which depends on the nature of the transition between the top of the valence band and bottom of conduction band. The lowest band gap energy in semiconducting materials is referred to as the fundamental absorption edge of inter-band transition and is characterized by m . For the allowed indirect transition $m = 1/2$, and for the allowed direct transition we have $m = 2$. Fig. 4 shows the band gap spectra of annealed and as-deposited CIAS thin films of different thicknesses. The value of optical band gap energy for increasing film thickness from 200 nm to 700 nm has been found to be decreased from 1.44 to 1.19 eV. In addition, annealing of the thin films improves their band gap value to 1.19 eV for 700 nm to 1.25 eV for 200 nm thin films. The reduction in the band gap and sharpening of the band edge at the band gap region clearly shows the improvement in the film uniformity after annealing. On the other hand, the density of localized state in the film increases with the film thickness, which leads to a decrease in the energy

band gap. In addition, the increase in particle size and decrease in strain and dislocation density may result in a reduction in band gap with increase of film thickness [20]. Many authors have reported such a variation in energy band gap with increase in film thickness [21]. However, a decrease in band gap of, less thick CIAS film, with annealing, is consistent with the fact that the crystallinity of the polycrystalline thin film improves on annealing [22]. Fig. 5 shows the clear difference in the band gap values before and after annealing.

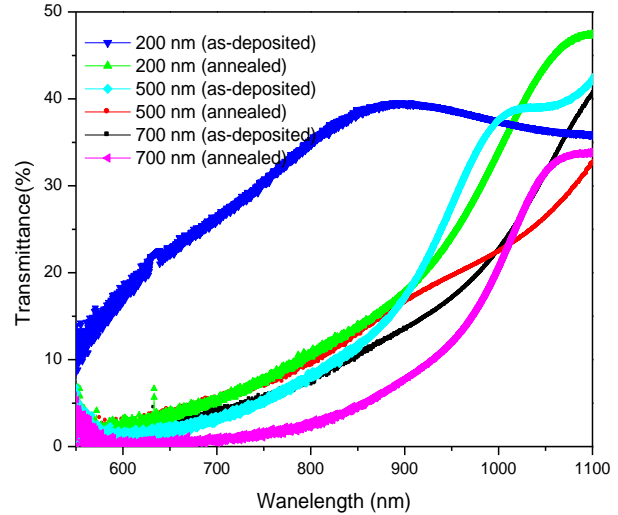


Fig. 3 – Optical transmission behavior of as-deposited and annealed CIAS thin films of different thicknesses

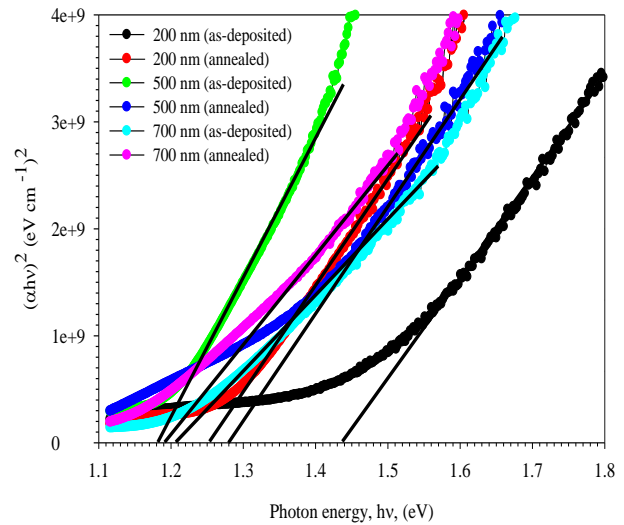


Fig. 4 – The energy band gap variation of as-deposited and annealed CIAS thin films of different thicknesses

Table 2 – The compositions of the as-deposited as well as annealed CIAS films as detected by the EDAX analysis

Element	Composition (wt. %)					
	700 nm (as-deposited)	700 nm (annealed)	500 nm (as-deposited)	500 nm (annealed)	200 nm (as-deposited)	200 nm (annealed)
Al K	6.54	6.59	2.70	5.15	3.25	3.73
Cu K	20.01	20.61	20.26	22.20	20.56	21.87
Se L	52.26	51.82	51.44	50.10	51.74	50.15
In L	21.19	20.98	25.60	22.55	24.45	24.61

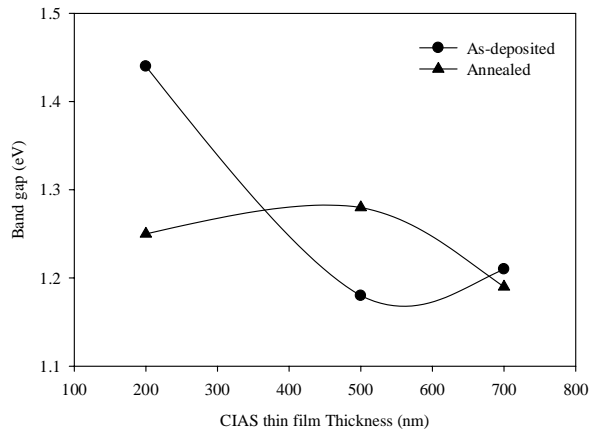


Fig. 5 - Variation of band gap (E_g) of as-deposited and annealed CIAS thin film of different thicknesses

It is observed that by annealing the CIAS films, the FWHM decreases while grain size increases. This increase in grain size results in a decrease of band gap as predicted by the following equation [23] and can be correlated with the XRD data

$$E_{(gap\ thin\ film)} = E_{(gap\ bulk)} + \pi^2 \hbar^2 / 8R^2 \times (1/m_e^* + 1/m_h^*) - 0.248 E_{RY}^* \quad (3)$$

where R is the radius of the grain size, m_e^* the effective mass of electron, m_h^* the effective mass of hole and E_{RY}^* the strain energy.

With increasing thickness as well as annealing, grain size increases, which results in the reduction of strain energy due to the rearrangement of the atoms. In this way, the grain boundaries are relaxed and eliminated. For thin films, the grains are under the influence of intrinsic stress that changes the optical properties of the film drastically. Stress is usually generated due to defects, as well as the substrate and thin film mismatch. The simple relationship between the intrinsic stress and grain size can be expressed by the following equation [24]:

$$\zeta = E_f \delta / \{(1 - \nu_f) D\} \quad (4)$$

where δ is the interaction potential across the grain boundaries, E_f Young's modulus, ν_f Poisson's ratio and D the grain size. From this equation, it is clear that as the grain grows and increases in size, the subsequent thin films tensile stress decreases. This is because as the grain grows, the grain boundaries that are relaxed are eliminated, the atoms are rearranged and the strain energy decreases. This will improve the optical characteristics of thin films [24].

3.5 Electrical Characterization

It has been observed that the resistivity decreases and the carrier concentration increases with the increase in film thickness as well as with annealing. These results show that the films with thickness of 700 nm exhibit the lowest resistivity and highest carrier concentration, thus, implying these are most conductive films. The decrease in resistivity with

increase in thickness as well as annealing has been interpreted on the basis of grain boundary scattering by Wu and Chiou [15]. It has been reported that as grain size increases with thickness and annealing, the effect of grain boundary is reduced, which, in turn, reduces the grain boundary scattering and increases the carrier lifetime, and, consequently, reducing the resistivity.

In addition, as per the grain-boundary carrier-trapping theory [25], these (grain boundaries) act as trapping centers and therefore hinder the transport of charge carriers towards the interface. For this reason, the density of grain boundaries should be low to reduce the recombination rate and improve the quality of the films and device performance. Thus, the improvement in the conductivity with thickness and annealing is due to the enhancement of grain size as seen in the XRD spectra and in SEM images. All the films exhibited p -type conductivity as determined on the basis of hot-probe method. The variation of resistivity and mobility with thickness for as-deposited as well as annealed CIAS layer is shown in Fig. 6.

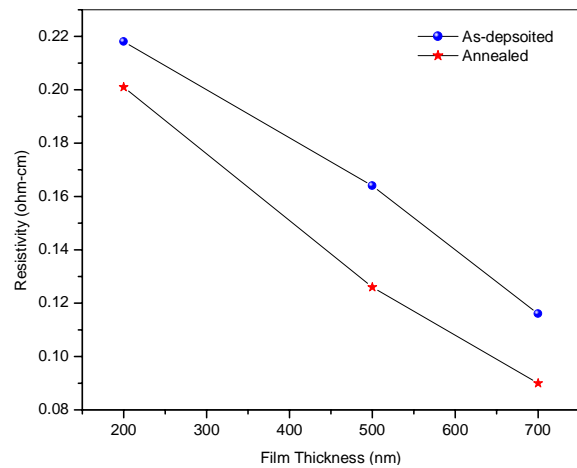


Fig. 6 - The resistivity variation of as-deposited and annealed CIAS thin films of different thicknesses

An optimization of the conditions of deposition of CIAS thin films with regard to their electrical response is required for their use in various device applications. Hall effect measurements of CIAS thin films deposited at 473 K having different thicknesses of as-deposited as well as annealed were carried out by using silver paste as a contact material and the results so obtained are presented in Table 3.

4. CONCLUSION

The grain sizes increased while strain and dislocation density decreased with increase in film thickness as well as with annealing. Increase in the film thickness and annealing has caused an increase in the electrical conductivity of the deposited films. Out of all deposited films, the films with a thickness of 700 nm exhibited the lowest resistivity, implying the most conductive films due to the highest carrier concentration. All the films exhibit p -type conductivity as depicted by hot-probe method. The decrease in resistivity with annealing can be explained by assuming that during the

Table 3 – Room temperature electrical properties of as-deposited and annealed CIAS thin films of different thicknesses

Thickness (nm)	Sample Type	Resistivity (Ω cm)	Mobility ($\text{cm}^2/\text{V}\cdot\text{s}$)	Carrier concentration (cm^{-3})
200	As-deposited	0.218	12.6	1.12E19
200	Annealed	0.201	17.2	1.54E19
500	As-deposited	0.164	22.2	2.2E19
500	Annealed	0.126	27.7	3.11E19
700	As-deposited	0.116	35.1	3.93E19
700	Annealed	0.090	37.2	7.71E19

annealing process, the films had enough time for atomic rearrangement within it. Further, films deposited at higher thicknesses exhibited comparatively low transmission and high absorbance in the visible region, the absorption further improved with annealing. The band gap decreases with increase in films thickness; however, the value further decreased on annealing; 700 nm thick annealed films were found as best suited for various device applications.

REFERENCES

- M.A. Conteras, B. Erasaas, K. Rmanathan, J. Hilner, A. Swartzlander, F. Hasoon, R. Noufi, *Prog. Photovolt. Res. Appl.* **7**, 311 (1999).
- Y. Hagiwara, T. Nakada, A. Kunioka, *Tech. Dig. 11th Photovolt. Sci. Eng. Conf.*, 83 (1999).
- T. Negami, Y. Hashimoto, S. Nishiwaki, *Tech. Dig. 11th Photovolt. Sci. Eng. Conf.*, 993 (1999).
- W.N. Shafarman, R. Klenk, B.E. McCandless, *J. Appl. Phys.* **79**, 7324 (1996).
- S. Marsillac, P.D. Paulson, M.W. Halmbodi, R.W. Birkmire, W.N. Shafarman, *Appl. Phys. Lett.* **81**, 1350 (2002).
- H.S. Ullal, K. Zweibel, B. von Roedern, *Proceedings of the 29th IEEE Photovoltaics Specialists Conference*, 472 (New Orleans, LA: USA: 2002).
- J.C.C. Fan, B.Y. Tsaor, B.J. Palm, *Proceedings of the 16th IEEE Photovoltaics Specialists Conference*, 692 (San Diego, CA: USA: 1982).
- U. Parihar, K. Sreenivas, J.R. Ray, C.J. Panchal, N. Padha, Bharati Rehani, *Mater. Chem. Phys.* **139**, 270 (2013).
- X.M. Fan, J.S. Lian, Z.X. Guo, *Appl. Surf. Sci.* **239**, 176 (2005).
- E.R. Shaaban, N. Afifyb, A. El-Tahera, *J. Alloy. Compound.* **482**, 400 (2009).
- C.S. Barrett, *Structure of Metals, Crystallographic methods, Principles and Data* (New York: McGraw-Hill: 1953).
- B.D. Cullity, *Elements of X-ray Diffraction* (USA: Addison-Wesley Publishing Company, Inc.: 1956).
- K.N. Tu, J.W. Mayer, *Electronic thin film Science for electrical Engineers and materials Scientists*, 7 (New York: Macmillan: 1992).
- P. Quintana, A.I. Oliva, *Superficies Vacio* **9**, 280 (1999).
- F. Wu, B.S. Chiou, *Appl. Surf. Sci.* **68**, 497 (1993).
- J.Y. Seto, *J. Appl. Phys.* **46**, 5247 (1975).
- Y. Masuda et al., *J. Korean Ceram. Soc.* **40**, 213 (2003).
- A.J. Moulson, *Electroceramics* (USA: 2nd Edition Wiley: 1990).
- G. Venkatarao, *J. Optoelectron. Adv. Mater.* **4**, 387 (2002).
- N.M. Shah, J.R. Ray, V.A. Kheraj, M.S. Desai, C.J. Panchal, B. Rehani, *J. Mater. Sci.* **44**, 316 (2009).
- Z.R. Khan, M. Zulfequar, M.S. Khan, *Chalcogenide Lett.* **431**, 7 (2010).
- N.M. Shah, J.R. Ray, K.J. Patel, V.A. Kheraj, M.S. Desai, C.J. Panchal, B. Rehani, *Thin Solid Films* **517**, 3639 (2009).
- A. Mahmood et al., *Phys. Scripta* **82**, 065801 (2010).
- Tsai K. Yue, T-S Han-Ping, D. Shieh, Ma C. Hsin, *J. Mater. Res.* **19**, 230614 (2009).
- B.A. Mansour, H. Shban, *J. Ovonic Res.* **6**, 13 (2010).

ACKNOWLEDGEMENTS

One of the authors (C.J. Panchal) also wish to thank "University Grants Commission" (UGC), New Delhi, India, for providing the financial assistance through major research project F. no. 40-448/2011 (SR) dated 4th July 2011.

This work was done in joint Ukraine-India scientific-technological project NoM/47-2013.